NASA TECHNICAL NOTE

NASA TN D-3829

NASA TN D-3829

EFFECT OF ORIFICE SIZE AND HEAT-TRANSFER RATE ON MEASURED STATIC PRESSURES IN A LOW-DENSITY ARC-HEATED WIND TUNNEL

by R. W. Guy and R. M. Winebarger

Langley Research Center
Langley Station, Hampton, Va.

NATIONAL AERONAUTICS AND SPACE ADMINISTRATION • WASHINGTON, D. C. • FEBRUARY 1967

NASA TN D-3829

EFFECT OF ORIFICE SIZE AND HEAT-TRANSFER RATE ON MEASURED STATIC PRESSURES IN A LOW-DENSITY ARC-HEATED WIND TUNNEL

By R. W. Guy and R. M. Winebarger

Langley Research Center
Langley Station, Hampton, Va.

NATIONAL AERONAUTICS AND SPACE ADMINISTRATION

For sale by the Clearinghouse for Federal Scientific and Technical Information
Springfield, Virginia 22151 – Price $2.00

EFFECT OF ORIFICE SIZE AND HEAT-TRANSFER RATE ON MEASURED STATIC PRESSURES IN A LOW-DENSITY ARC-HEATED WIND TUNNEL

By R. W. Guy and R. M. Winebarger
Langley Research Center

SUMMARY

An experimental investigation of the effect of orifice diameter and heat-transfer rate on static-pressure measurements has been made in the flow region between continuum and free molecule. Heat-transfer and pressure measurements were obtained over a range of tunnel test conditions with Mach number varying from 12.2 to 14.1, total enthalpy varying from 3.07 to 4.95 MJ/kg (1320 to 2130 Btu/lbm), free-stream Reynolds number varying from 400 to 889 per centimeter (1.22×10^4 to 2.71×10^4 per foot) and free-stream mean-free-path length varying from 0.234 to 0.452 mm (0.0092 to 0.0178 inch). The experimental results for the orifice effect are general when presented in terms of parameters from a previously existing theory, even though the present data were obtained on a slightly blunted 10^o semivertex angle cone.

The present tests, which were conducted in both air and nitrogen, extend the range of experimental data obtained on the orifice effect under actual flow conditions. This is true since the present data were obtained at higher heat-transfer rates at the density level involved than previous flow data. The trend in the data was the same for both gases and, generally, good agreement with experiment was obtained when Potter's semiempirical theory was used for the orifice effect.

The pressure data taken with heat transfer to the model showed a significant decrease in measured pressure with a decrease in orifice diameter. The results show that the proper size orifice to use in a particular situation will depend on both the density level and the heat-transfer rate. In many cases, it may be more practical to use a conveniently sized orifice and correct the pressure data by use of Potter's semiempirical theory rather than to try to eliminate this effect by choice of orifice size. However, the orifice effect should be considered in experimental pressure data obtained in low-density flow with heat transfer.

INTRODUCTION

The use of orifices to measure pressures in the region between continuum and free molecule flow has been shown by several theoretical and experimental investigations to be complicated by a number of phenomena. Some of the phenomena which have received attention are pressure-measuring system response time (refs. 1 and 2), outgassing (ref. 2), thermal creep (refs. 2 to 6), and momentum mixing (refs. 7 and 8).

Pressure measurements are also affected by heat-transfer rate and orifice diameter in the region between continuum and free molecule flow. According to Potter et al. (ref. 9), this phenomenon is caused by the existence of unequal speed distributions between incoming and outgoing molecules in the orifice entrance region and is evidenced by a decrease in measured pressure with a decrease in orifice diameter for a given density level and heat-transfer rate. Bailey and Boylan (ref. 10) and Bailey (ref. 11) showed the existence of this phenomenon with measurements taken with impact pressure probes. Potter et al. (ref. 9) suggested that the phenomenon be termed "orifice effect" and presented a semiempirical theory for the orifice effect which bridges the gap between continuum and free molecule flow. Vidal and Bartz (ref. 12) also noted the existence of an "orifice effect" and treated the phenomenon in a manner similar to Knudsen's treatment of thermal creep by using a gas temperature which is dependent on the heat-transfer rate. More recently, Deskins and Boylan (ref. 13) have investigated the effect of orifice shape in rarefied flow with heat transfer.

The orifice effect was the subject of the present investigation. The authors noted that the static pressures measured on some slender cones during a preliminary investigation of viscous-induced pressures fell considerably below theory. A search for the cause of the low measured pressures indicated that the orifice effect might be a primary factor.

The experimental investigation was undertaken to extend the range of experimental data on the orifice effect under actual tunnel flow conditions. The present data were obtained at higher heat-transfer rates at the density level involved than previous flow data. Another purpose of the investigation was to determine the orifice effect on measured static pressures in both air and nitrogen. Also, the data were expected to provide essential information for the improvement of pressure-measuring technique and to provide a more rigorous test of Potter's semiempirical theory than had previously been true.

The model used in the tests was a 10° semivertex angle cone with a 3.18-mm (0.125-inch) diameter plane, blunt tip. Seven circular orifices with diameters ranging from 0.64 mm (0.025 inch) to 2.69 mm (0.106 inch) and located around the circumference of the cone at a single axial location were used to determine the orifice effect on the measured pressures. Alinement orifices located at this same axial position were used to aline the model with the flow. A cone was chosen for the investigation because once the model

was alined with the stream, any variation of pressure around the circumference of the cone could be due only to orifice size.

This investigation was conducted in the Langley 1-foot (0.305-meter) hypersonic arc tunnel using both air and nitrogen as the working media. The free-stream Mach number ranged from 12.2 to 14.1, the free-stream Reynolds number ranged from 400 to 889 per centimeter (1.22×10^4 to 2.71×10^4 per foot), total enthalpy ranged from 3.07 to 4.95 MJ/kg (1320 to 2130 Btu/lbm), and free-stream mean-free-path length ranged from 0.234 to 0.452 mm (0.0092 to 0.0178 inch).

SYMBOLS

A percent of p_{io}

$$B = \frac{\dot{q}_w N_{Pr,w}(\gamma - 1)}{0.8512\gamma(RT_w)^{0.5}}$$

C constant of maximum pressure variation, see equation (A1)

d orifice diameter

$$D = \left(0.071 \frac{d}{\lambda_c} + 1.068\right)^{2.95}$$

h static enthalpy

H_t total enthalpy

k thermal conductivity

$$K_w = \frac{\dot{q}_w N_{Pr,w}(\gamma - 1)}{\gamma p_i (RT_w)^{0.5}}$$

t wall thickness

M Mach number

N_{Pr} Prandtl number

$N_{Re,\infty}$	free-stream Reynolds number per unit length
p	pressure
p'	measured pressure uncorrected for misalinement
p_i	measured pressure corrected for misalinement
p_{io}	true pressure, that is, pressure on the surface outside the orifice (ref. 9)
$\bar{p}$	normalized pressure, $\dfrac{p_i/p_{io} - \left(p_i/p_{io}\right)_L}{1 - \left(p_i/p_{io}\right)_L}$
Δp_{mm}	pressure increment due to momentum mixing
$\dot{q}$	heat-transfer rate
R	specific gas constant
T	temperature
ΔT	temperature differential across the wall in instrumentation plane
V	velocity
x	distance along cone surface from blunt tip
δ	calculated misalinement angle (approximate value)
γ	ratio of specific heat at constant pressure to specific heat at constant volume
θ_c	cone semivertex angle
λ	mean free path, $\left(\dfrac{\pi}{2RT}\right)^{1/2} \dfrac{\mu}{\rho}$

μ coefficient of viscosity $\left(\text{after Sutherland, } \mu = 2.27 \frac{T^{3/2}}{T + 198.6} \times 10^{-8}, \text{ lbf-sec/ft}^2 \text{ with } T \text{ in } {}^{\circ}R\right)$

ρ density

ϕ angular location around cone circumference (see fig. 1)

ϕ_m angular location of most windward ray of cone

Subscripts:

A alinement orifice

c based on T_w and p_{io} (ref. 9)

c,i based on T_w and p_i (ref. 9)

L limit as $\lambda_c/d \to \infty$ (ref. 9)

t,1 total conditions in free stream

t,2 total conditions behind normal shock

w wall condition

∞ free stream ahead of shock

APPARATUS AND TESTS

Tunnel and Test Conditions

The present investigation was conducted in the Langley 1-foot (0.305-meter) hypersonic arc tunnel, a description of which can be found in reference 14. Both air and nitrogen are commonly used as test media.

The tests were made over a Mach number range from 12.2 to 14.1, a free-stream unit Reynolds number range from 400 to 889 per centimeter (1.22×10^4 to 2.71×10^4 per foot), and a stagnation enthalpy range from 3.07 to 4.95 MJ/kg (1320 to 2130 Btu/lbm). The free-stream mean-free-path length varied from 0.234 to 0.452 mm (0.0092 to

0.0178 inch). All tunnel test conditions are presented in table I along with the measured heat-transfer rates and ratios of wall enthalpy to stagnation enthalpy in the instrumentation plane of the model. Test times for the present investigation were 4 minutes.

Model

The model used in the tests was a water-cooled, sting-supported, 10° semivertex angle cone with a 3.18-mm (0.125-inch) diameter plane, blunted tip and a 5.08-cm (2.00-inch) base diameter. Model wall material was 347 stainless steel with a thickness of 2.41 mm (0.095 inch).

A schematic of the model and a table showing instrumentation locations are presented in figure 1. The instrumentation plane contained nine orifices, three of which had the same diameter. Thus, seven orifices with different diameters were used to investigate the orifice effect. The three orifices with the same diameter were used to aline the model and to provide a means of correction for any small misalinement effect. All orifices were round, burrs and protuberances being removed.

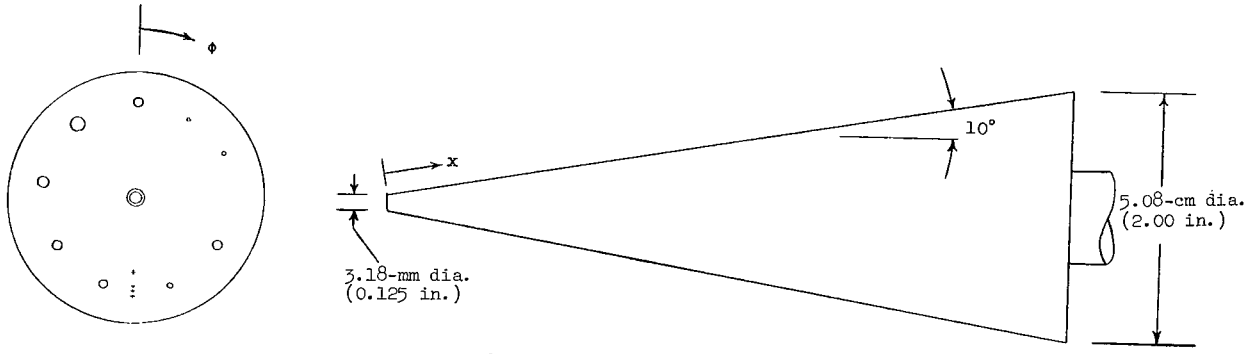

Pressure orifices* at x = 9.90 cm (3.90 in.)		
ϕ, deg	d	
	mm	in.
0	1.70	0.067
30	.64	.025
60	.76	.030
120	1.70	.067
160	1.14	.045
200	1.50	.059
240	1.70	.067
280	2.21	.087
320	2.69	.106
Tip	2.57	.101

*x = 0 at tip.

Thermocouples at ϕ = 180°		
x		Type
cm	in.	
7.62	3.00	Chromel-alumel
9.27	3.65	Chromel-alumel
9.90	3.90	Copper-constantan
9.90	3.90	Copper-constantan*
10.55	4.15	Chromel-alumel

*Mounted on interior surface.

Figure 1.- Orifice effects model schematic and instrumentation table.

Instrumentation

The instrumentation plane contained two insulated, metal-sheathed, copper-constantan thermocouples; one to measure surface temperature and the other to measure the inside wall temperature. The output from these thermocouples was recorded on a continuous recording potentiometer. Accuracy of these temperature measurements based on the manufacturer's quoted accuracy and the possible reading error, was $\pm 0.7^{\circ}$ K ($\pm 1.26^{\circ}$ R).

Chromel-alumel thermocouples were located along the surface of the model to measure the surface temperature distribution in the vicinity of the instrumentation plane. These thermocouples were also insulated and metal-sheathed. The output from these thermocouples was recorded on an 18-channel oscillograph. The accuracy of these temperature measurements was $\pm 1.4^{\circ}$ K ($\pm 2.5^{\circ}$ R).

The smaller diameter orifice tubing was stepped up to larger diameter tubing in as short a length as possible to minimize pressure lag time. Orifice tubing with diameters ranging from 0.64 to 1.70 mm (0.025 to 0.067 inch) was 1.40 cm (0.55 inch) in length followed by 1.52 meter (5 feet) of 2.38 mm (0.0938 inch) inside diameter step-up tubing. The 2.21 mm (0.087 inch) diameter and the 2.69 mm (0.106 inch) diameter tubing was not stepped up and was 1.52 meter (5 feet) in length.

Pitot and cone static pressures were measured with ionization gages which employ a radioactive source to ionize the gas sample within the gage volume (1.57 cm^3 or 0.096 in^3). These gages have ranges of 0 to 400 N/m^2 (0 to 3 mm Hg) and 0 to 4000 N/m^2 (0 to 30 mm Hg). Manufacturer's quoted accuracy is ± 2 percent of the reading from 133.3 to 4000 N/m^2 (1 to 30 mm Hg) and ± 5 percent of the reading from 13.3 to 133.3 N/m^2 (0.1 to 1 mm Hg). No accuracy is quoted for pressures less than 13.3 N/m^2 (0.1 mm Hg). More information on this type of gage may be found in reference 15. Outputs from these ionization gages were amplified and recorded on the 18-channel oscillograph.

Calibration and Test Procedure

The ionization gages were calibrated against a McLeod gage which had been outgassed and checked for the presence of condensables. A typical ionization gage calibration is shown as figure 2. The gages were found to hold calibration very well. Repeatability between the individual gages was found to be about 2 percent at the pressure level of the present tests, about 40 N/m^2 (0.300 mm Hg).

The ionization gages were kept at a pressure of about 0.67 N/m^2 (0.005 mm Hg) except during tests and calibrations to insure cleanliness of the gages and the associated tubing. Prior to a test, the pressure gages were overpressured to approximately

1333 N/m^2 (10 mm Hg) with dry air. Once flow was fully established, the gages were connected to the model pressure tubing by the use of solenoid valves. After allowing sufficient time for the pressures to settle out and for the taking of data, the gages were again switched to a controlled environment and the flow was stopped.

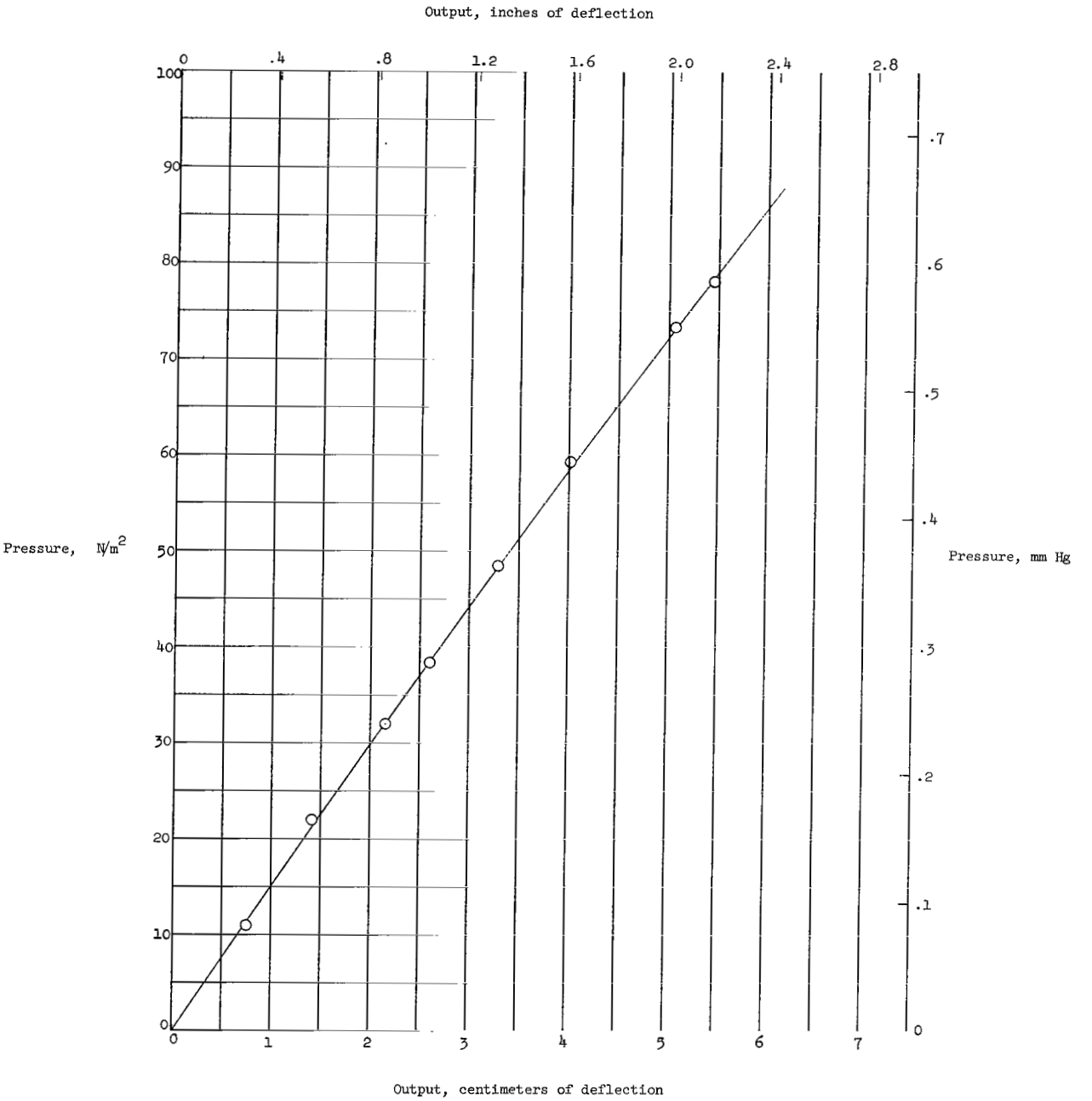

Figure 2.- Typical ionization gage calibration curve.

The first tests of the series were used to find the approximate angle of the model with respect to the flow and the model was then realined. Some variation of the misalinement angle occurred from test to test because of small movements of the model while preparing for the next test. However, the misalinement angle was held to a minimum, generally less than 0.25°, to avoid masking of the orifice effect.

DATA REDUCTION

Pressures

Although the readings from alinement orifices generally agreed within the accuracy of the gages and readout capability, a correction for misalinement was applied in all cases where there was any disagreement between the reading of the alinement orifices. The method of correction is presented in appendix A. This correction smoothed the data and, in all cases, the trend of the corrected data was better than that of the uncorrected data. The consistency of the results of the misalinement correction seems to justify its use.

The experimental pressure data both uncorrected and corrected for model misalinement are presented in table II. Also presented in this table is the angular location of the most windward conical ray and the approximate misalinement angle. This misalinement angle was calculated by using the results of reference 16 and $p_{i,A}$ and M_{∞} for a given test.

Heat Transfer

The copper-constantan thermocouples located on the inside and outside surfaces of the model in the instrumentation plane were used to determine ΔT across the wall. Steady-state heat transfer was calculated from

$$\dot{q}_w = -k \frac{\Delta T}{t} \tag{1}$$

The wall thickness t was measured with a micrometer and was 2.41 mm (0.095 inch). The value of thermal conductivity k used was based on a temperature of 310° K (558° R) which is an average of all inside and outside surface temperatures for all tests. At 310° K (558° R) the thermal conductivity of 347 stainless steel is 14.45 J/s-m-$^{\circ}$K (8.35 Btu/hr-ft-$^{\circ}$R) (ref. 17).

Accuracy

The maximum possible error involved in the measured static pressures is based on ±5 percent of the gage reading as quoted by the manufacturer of the ionization gages and the reading error involved in reading the oscillograph tapes. The maximum possible

error was ±9 percent on test 1, ±7 percent on tests 2 to 9 and tests 14 and 15, and ±6 percent on tests 10 to 13 and tests 16 and 17.

It is believed, however, that the actual gage error is less than ±5 percent of the reading. Repeat calibrations of the ionization gages indicate that the gages used could be quoted as having an accuracy of ±2.5 percent of the reading. The smoothness of the present data also tends to confirm that the gages were better than quoted by the manufacturer.

No attempt was made to describe quantitatively the error in the quoted heat-transfer rates because it was not possible to obtain the degree of accuracy of all parameters involved in the heat-transfer computation. However, ΔT was measured with a possible error of $\pm 1.4^{\circ}$ K (2.5° R). A consideration of the possible errors involved in the heat-transfer measurements indicates that these errors would probably tend to make the measured heat-transfer rates lower than the actual values.

Theory

The theory of the orifice effect in free molecular flow as well as a description of the experiment which led to Potter's semiempirical theory may be found in reference 9. A working chart for the correction of the orifice effect, which presents p_i/p_{io} as a function of $d/\lambda_{c,i}$ and K_w, was given in reference 9. However, in order to compare the present experimental data with Potter's semiempirical theory, it became necessary to extend the semiempirical theory to lower values of K_w. Details of this extension as well as a brief review of the cause of the orifice effect are presented in appendix B.

The expression developed for the true pressure on the surface outside the orifice is

$$p_{io} = \frac{p_i + B - \frac{B}{D} + \sqrt{\left(\frac{B}{D} - B - p_i\right)^2 - 4p_iB}}{2} \tag{2}$$

which is equation (B9) of appendix B. The known quantities in equation (2) are p_i and B, whereas p_{io} and D are unknown. Consequently, equation (2) is solved by iteration using $d/\lambda_{c,i}$ as a first choice of d/λ_c in the calculation of D. Convergence to the correct values of p_{io} and d/λ_c is rapid.

This iteration procedure was used to reduce the present data. For a given test, p_{io} for each orifice was obtained from equation (2) and these p_{io} values from the different sized orifices were averaged to get an average p_{io} for the test. This $(p_{io})_{\text{theory av.}}$ was then used to nondimensionalize the experimental data and to determine the theoretical values of p_i for comparison with experiment by use of

$$p_i = \frac{Bp_{io}}{D\left(p_{io} - B\right)} + p_{io} \tag{3}$$

Equation (3) is developed in appendix B as equation (B10).

Figure 3 represents an extended orifice effect correction chart. This chart was derived from the following equation:

$$K_w = 0.8512 \frac{p_{io}}{p_i}\left[1 - \frac{1}{1 + \left(0.071 \frac{d}{\lambda_{c,i}} \frac{p_{io}}{p_i} + 1.068\right)^{2.95}\left(\frac{p_i}{p_{io}} - 1\right)}\right] \tag{4}$$

which is also derived in appendix B as equation (B15). By choosing a range of p_i/p_{io}, equation (4) was used to calculate a range of K_w for a given value of $d/\lambda_{c,i}$.

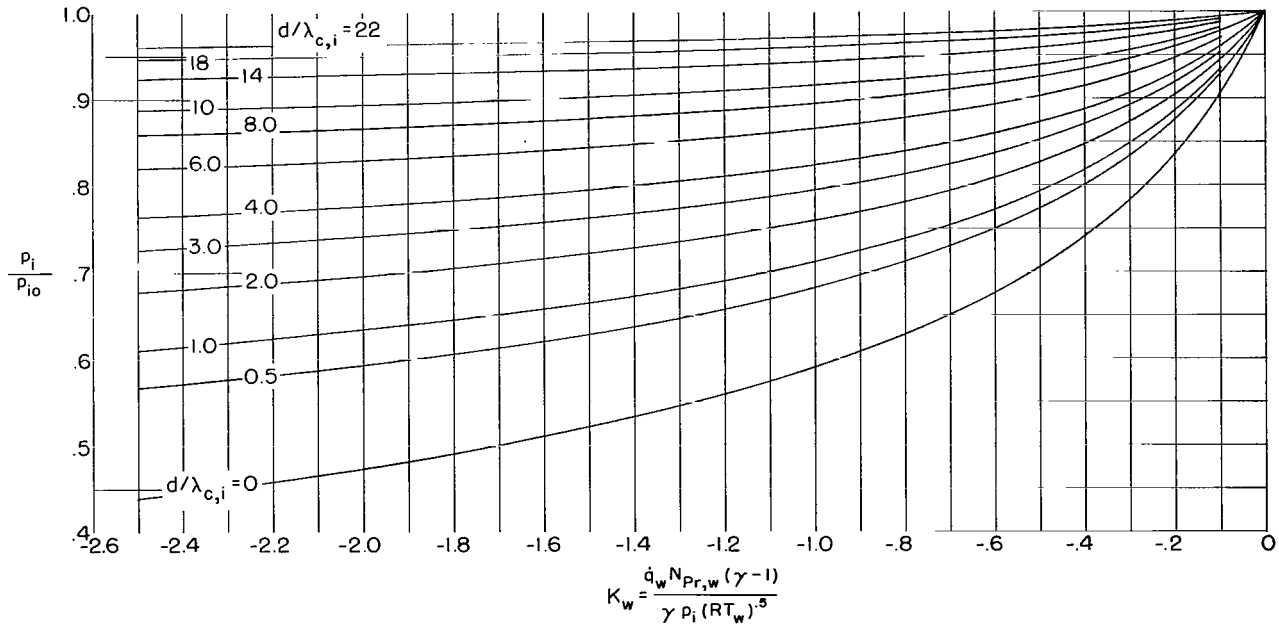

Figure 3.- A working chart for the correction of the orifice effect. (This figure was derived directly from data presented in ref. 9 and represents an extension of fig. 11 of ref. 9.)

RESULTS AND DISCUSSION

The measured pressures, both corrected and uncorrected for misalinement have been presented in table II. All the data taken with heat transfer to the model showed a significant decrease in measured pressure as orifice size decreased.

Several factors in addition to the orifice effect can affect the measurement of pressure in the region between continuum and free molecule flow. Thus, it was necessary to consider the possible effects on the pressure data of lag time, outgassing, thermal creep, and momentum mixing so that the orifice effect could be isolated as much as possible.

Lag time was computed for the pressure-measuring system used in the present tests by the method of reference 1 at the pressure levels that were expected during the tests. Also, a lag-time experiment was conducted with the system that was used in the tests. Results indicated that the pressures were not changing to any significant degree after 4 minutes of settle-out time; however, the smaller orifices would no doubt have settled out further if much more time had been allowed.

As mentioned previously, the ionization gages were overpressured prior to a test so that during a test, the pressure decayed to the measured value. In the presence of any lag-time effects, the smaller orifices would have been indicating a higher reading than would be the case with no lag time effects; thus, any small lag time effect would tend to make the orifice effect appear on the conservative side.

Outgassing was not considered to be a serious problem during the present tests since the ionization gages and the associated tubing were held at a pressure of about 0.67 N/m^2 (0.005 mm Hg) at all times except during tests and calibrations. The model pressure tubing was also held at a pressure level considerably below the test pressure for some time prior to a test.

The problem of thermal creep due to a temperature gradient along the pressure tubing was of no significance during the present tests, according to the working correction chart presented in reference 6. This was true because the gradient along the orifice tubing was such that the ratio of the hot-end temperature to the cold-end temperature never exceeded 1.07 and the maximum correction would be 2 percent.

The effect of momentum mixing (shown, for example, in refs. 7 and 8) on the pressure data is more difficult to analyze. Talbot (ref. 7) suggested that the effect might be a "ram" effect (dependent on Mach number) and not a viscous effect nor a rarefaction phenomenon associated with large mean free path. Talbot presented a correlation attempt for the pressure rise due to momentum mixing as

$$\Delta p_{mm} = 81.4\sqrt{M_\infty}d \tag{5}$$

where Δp_{mm} is in N/m^2 and d is in meters.

Since no experimental data or theory on momentum mixing are known to exist for conditions similar to those of the present tests, equation (5) was used as a guide for the possible magnitude of the effects of momentum mixing on the present pressure data. Thus, according to equation (5), any effect of momentum mixing on the data would be too small to be determined within the accuracy of the pressure measurements. In addition, it seems that the orifice effect would overshadow the momentum mixing effect and the two would be very difficult to separate. Figure 4(b) tends to show that no effect of momentum mixing can be discerned within the accuracy of the present data, since there is no trend toward an increase of measured pressure with orifice diameter. In this case, the orifice effect should be nonexistent since the heat-transfer rate is zero.

After a consideration of the preceding factors which might have affected the pressure data, it seems safe to assume that the effect noted during the present tests is due primarily to the orifice effect.

A comparison of figures 4(a) and 4(b) illustrates the effect of heat-transfer rate on the experimental pressure data. The bars on the data that are uncorrected for misalinement indicate the maximum possible error in the pressure measurements as discussed earlier.

Figure 4(a) is a "hot" test in air at a high enthalpy with heat transfer to the model. Note that the orifice effect is considerable, the measured pressures varying from 29.1 to 40.1 N/m^2 (0.218 to 0.301 mm Hg) over an orifice diameter range from 0.64 to 2.69 mm (0.025 to 0.106 inch). Potter's semiempirical theory agrees very well with the experimental data.

Figure 4(b) is data taken under "cold" flow conditions (room temperature air at 61 N/cm^2 (6.0 atm) stagnation pressure expanded in the nozzle) with essentially zero heat transfer. No effect of orifice size is evident in the pressure data taken under conditions with no heat transfer to the model.

No approximate misalinement angle is quoted for test 1 because of the uncertainty of Mach number for this "cold" flow. Other test section conditions are also uncertain because of the possible existence of such phenomena as supercooling and liquefaction of the air. However, a flow-visualization technique using an electron beam (ref. 18) has established the existence of supersonic flow under these "cold" flow conditions.

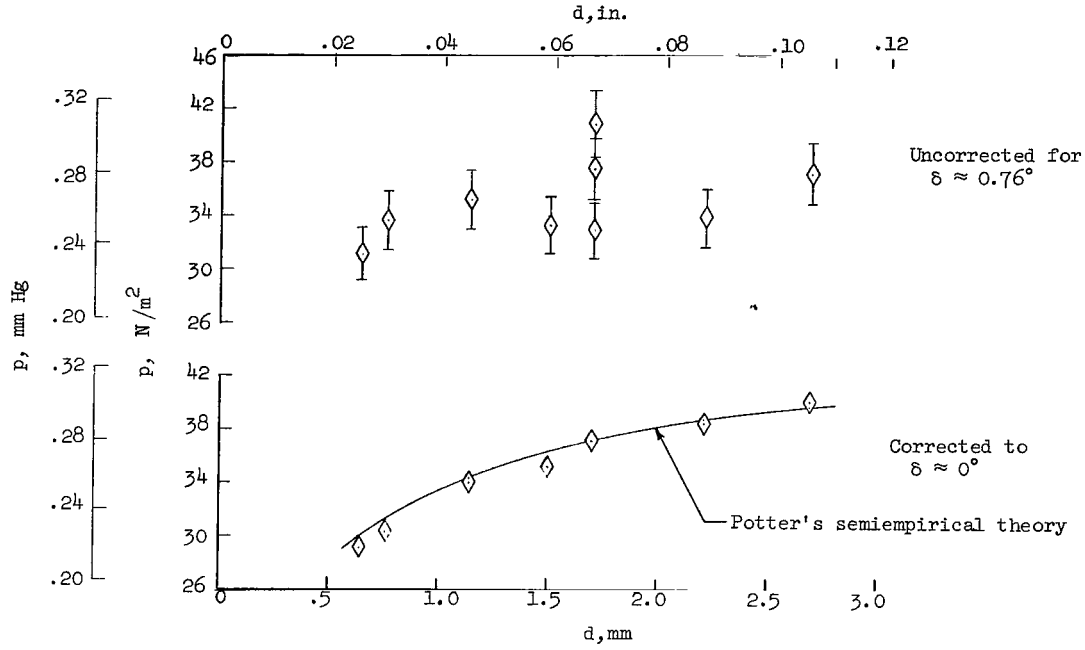

(a) Test 7; air; $\dot{q}_w = -9.45 \frac{J}{cm^2 s} \left(-8.32 \frac{Btu}{ft^2\text{-}sec}\right)$.

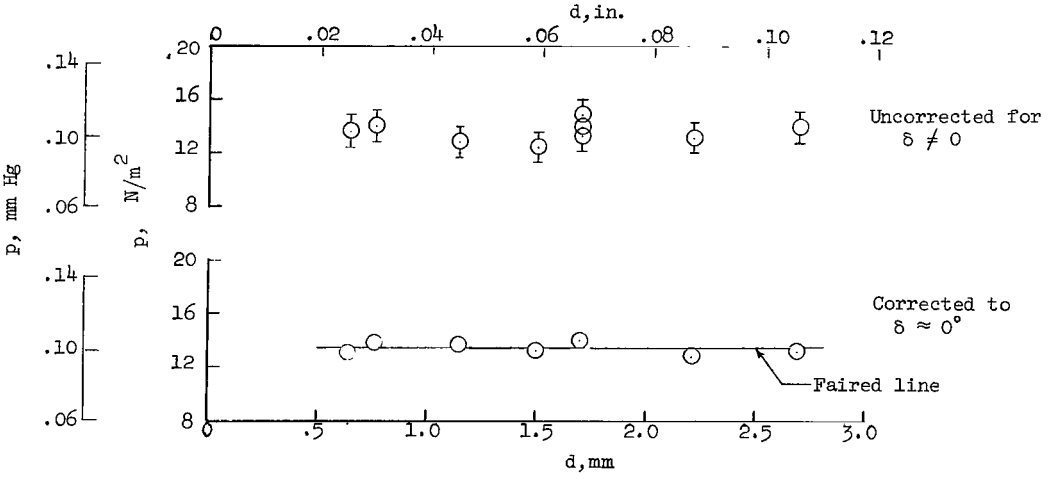

(b) Test 1; air; $\dot{q}_w \approx 0$.

Figure 4.- An illustration of the influence of heat-transfer rate on measured pressures in low-density flow.

Figures 5(a) and 5(b) illustrate the importance of heat-transfer rate in using Potter's semiempirical theory to predict the measured pressures. As $\dot{q}_w$ increases at a certain density level, the effect on the measured pressures diminishes and tends to a limit.

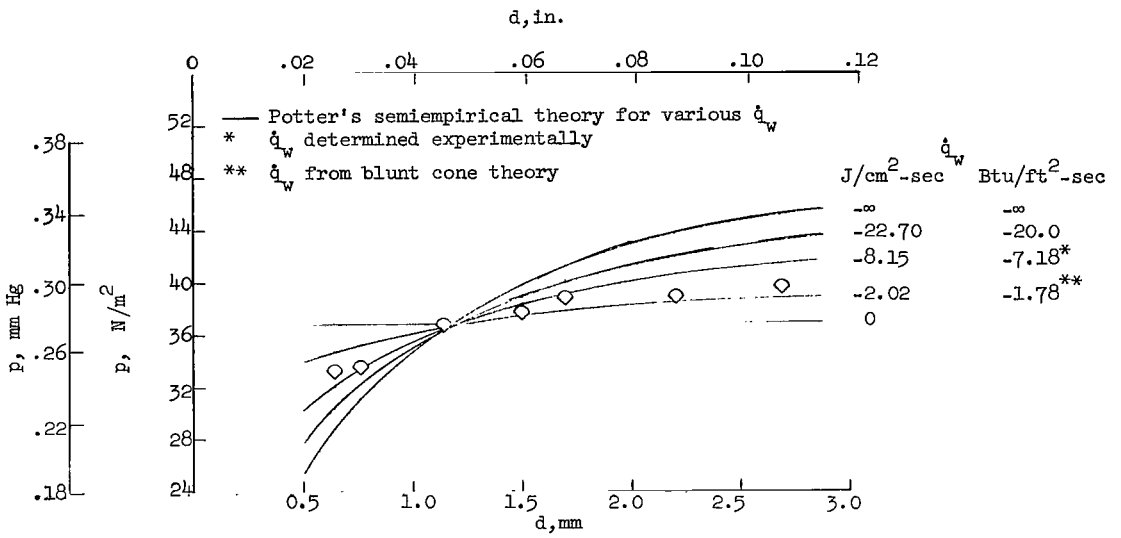

(a) Test 8; air.

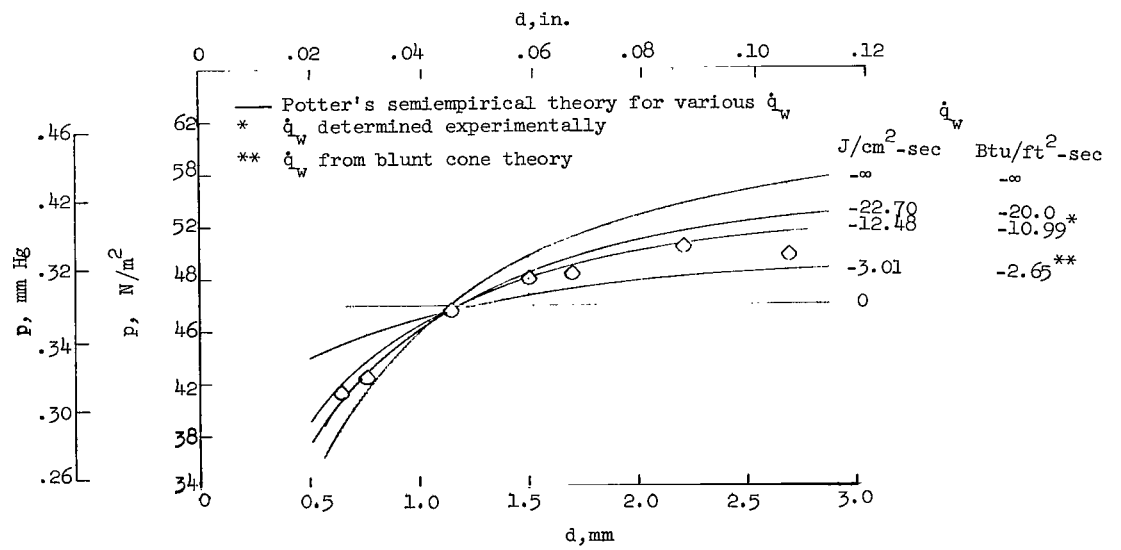

(b) Test 13; air.

Figure 5.- Measured pressures compared with theoretical predictions for various heat-transfer rates.

In the present tests, the experimentally determined heat-transfer rate in the instrumentation plane was always higher than the theoretical value, even when corrections for induced pressure effects and transverse curvature were added to the theoretical blunt-cone estimate. In virtually all cases, however, better agreement between Potter's theory and the measured pressures is obtained by using the experimental values of heat transfer.

Figure 6 is a comparison of the predicted and the experimentally determined orifice effect on pressure measurements in both air and nitrogen. An attempt was made to

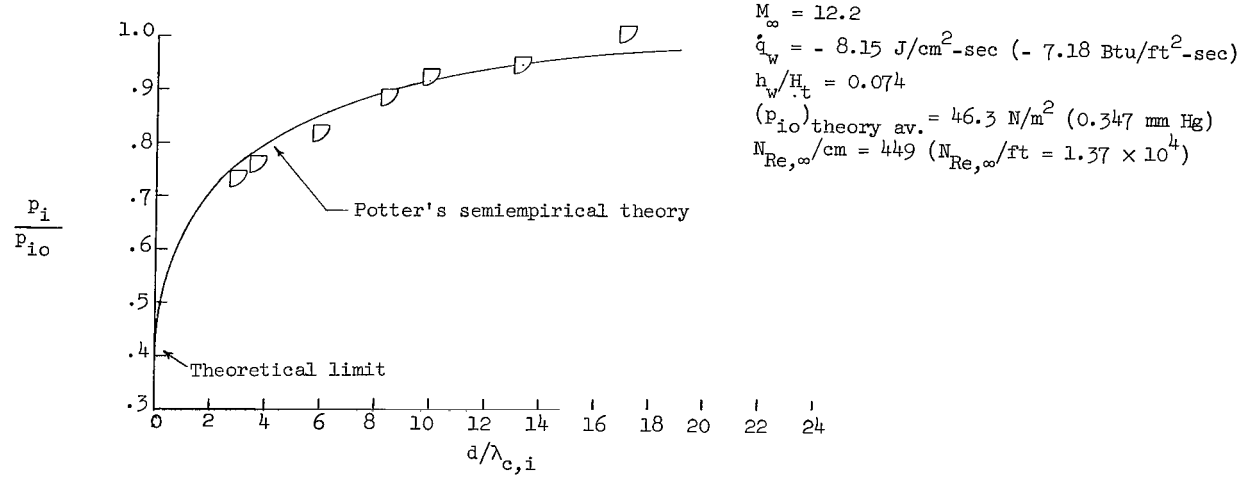

(a) Test 5; air.

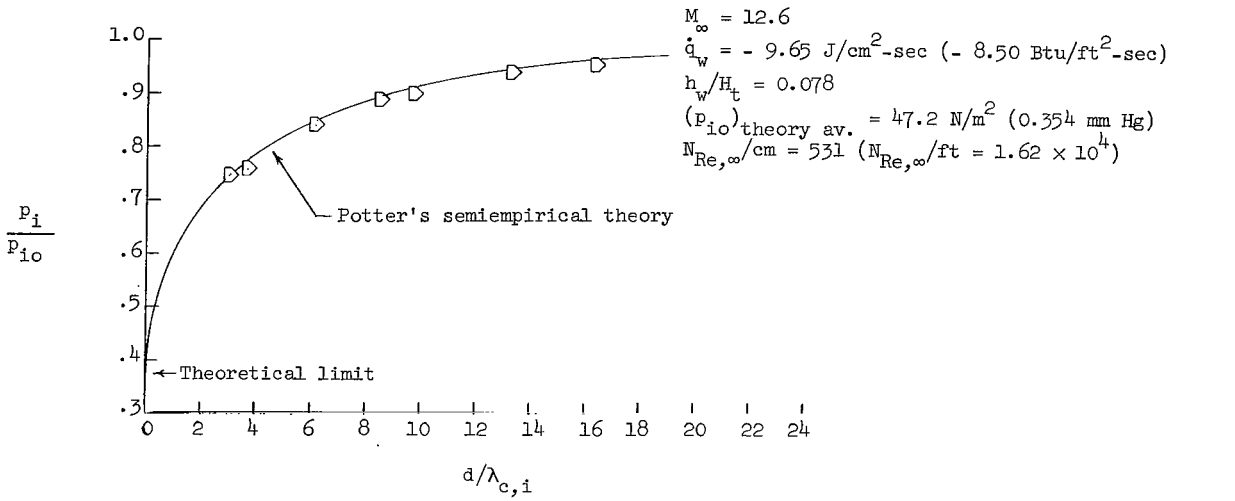

(b) Test 12; air.

Figure 6.- Comparison of predicted and experimental orifice effect.

present a cross section of the data by presenting one of the poorest and one of the best cases of agreement with theory in both gases. In all cases, however, Potter's semi-empirical theory is adequate.

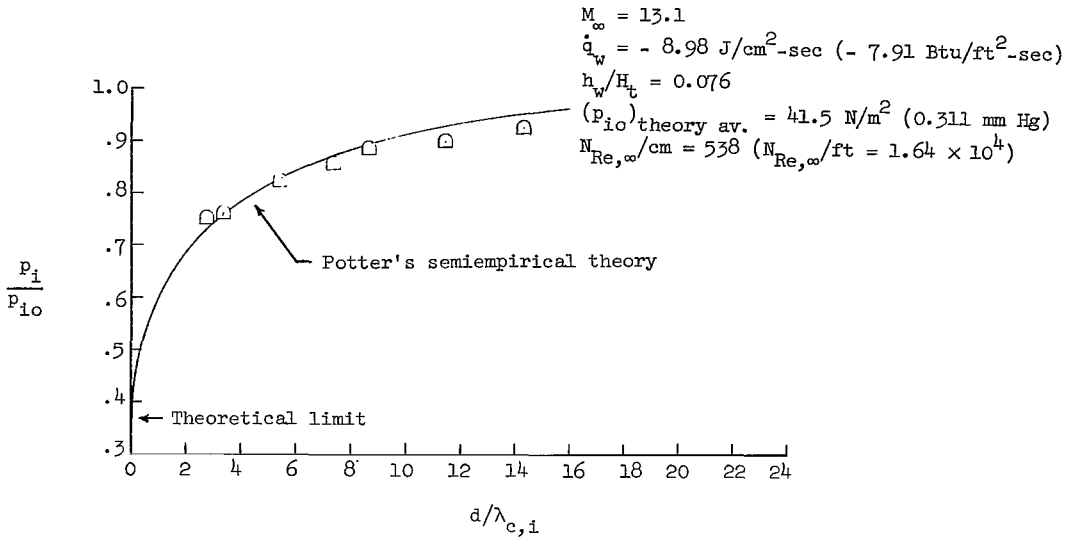

(c) Test 15; nitrogen.

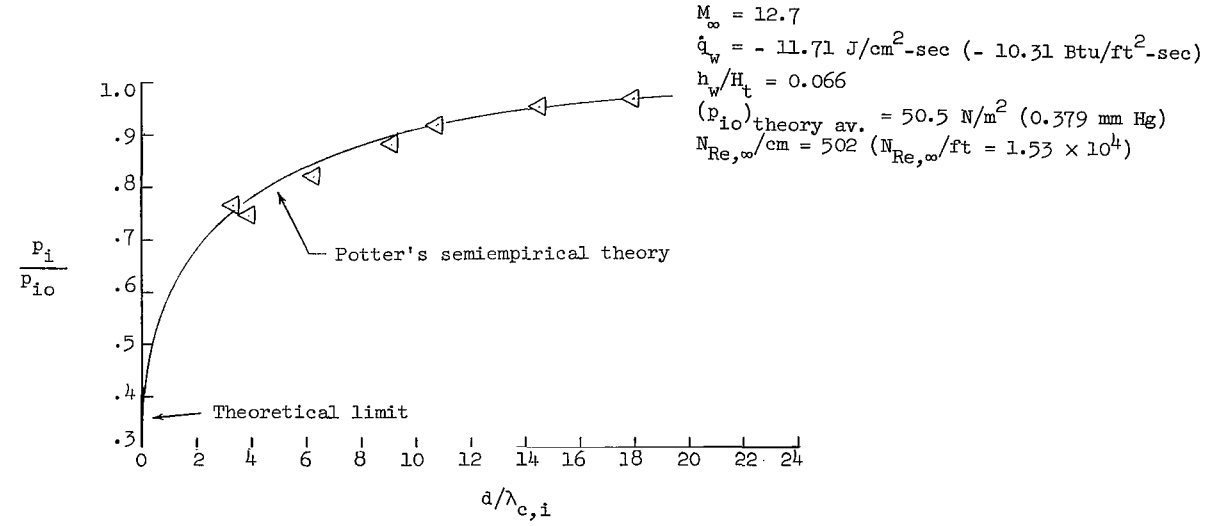

(d) Test 16; nitrogen.

Figure 6.- Concluded.

All the pressure data obtained during the present tests are shown in figure 7 as p_i/p_{io} plotted against $d/\lambda_{c,i}$. These data should form a band rather than a single curve since both heat-transfer rate and pressure level varied to some extent from test to test. The severity of the orifice effect depends directly on $\dot{q}_w$ and inversely on p_i and T_w,

Symbol	Test	$(p_{io})_{theory\ av.}$		$\dot{q}_w$	
		N/m^2	mm Hg	J/cm^2-s	$\frac{Btu}{ft^2\text{-sec}}$
Air					
□	2	40.7	0.305	-8.09	-7.12
△	3	46.4	.348	-6.72	-5.92
◇	4	46.8	.351	-6.39	-5.63
▽	5	46.3	.347	-8.15	-7.18
◁	6	40.8	.306	-7.42	-6.53
◆	7	41.6	.312	-9.45	-8.32
▽	8	43.2	.324	-8.15	-7.18
◁	9	44.8	.336	-9.31	-8.20
▼	10	44.3	.332	-8.72	-7.68
◇	11	45.7	.343	-9.72	-8.56
▷	12	47.2	.354	-9.65	-8.50
△	13	54.9	.412	-12.48	-10.99
Nitrogen					
▷	14	39.7	0.298	-4.83	-4.25
▷	15	41.5	.311	-8.98	-7.91
◁	16	50.5	.379	-11.71	-10.31
◁	17	40.3	.302	-8.38	-7.38

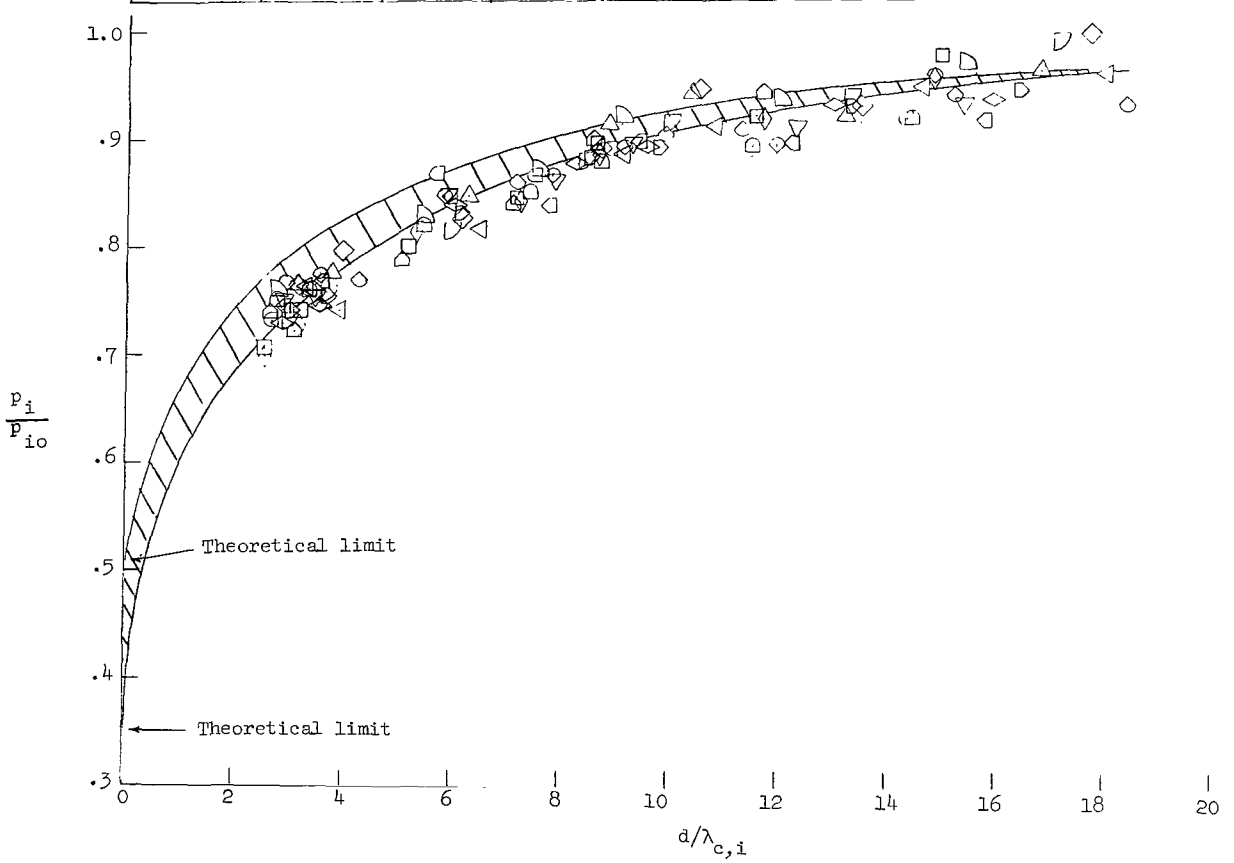

Figure 7.- Comparison of all experimental data with theoretical band. $T_w \approx 320^0$ K (576^0 R).

Symbol	Test	$(p_{io})_{theory\ av.}$ N/m²	$(p_{io})_{theory\ av.}$ mm Hg	$\dot{q}_w$ J/cm²-s	$\dot{q}_w$ Btu/ft²-sec
		Air			
□	2	40.7	0.305	-8.09	-7.12
△	3	46.4	.348	-6.72	-5.92
◇	4	46.8	.351	-6.39	-5.63
▷	5	46.3	.347	-8.15	-7.18
◻	6	40.8	.306	-7.42	-6.53
◇	7	41.6	.312	-9.45	-8.32
◁	8	43.2	.324	-8.15	-7.18
▽	9	44.8	.336	-9.31	-8.20
◇	10	44.3	.332	-8.72	-7.68
▷	11	45.7	.343	-9.72	-8.56
◇	12	47.2	.354	-9.65	-8.50
	13	54.9	.412	-12.48	-10.99
		Nitrogen			
▷	14	39.7	0.298	-4.83	-4.25
◻	15	41.5	.311	-8.98	-7.91
◁	16	50.5	.379	-11.71	-10.31
△	17	40.3	.302	-8.38	-7.38

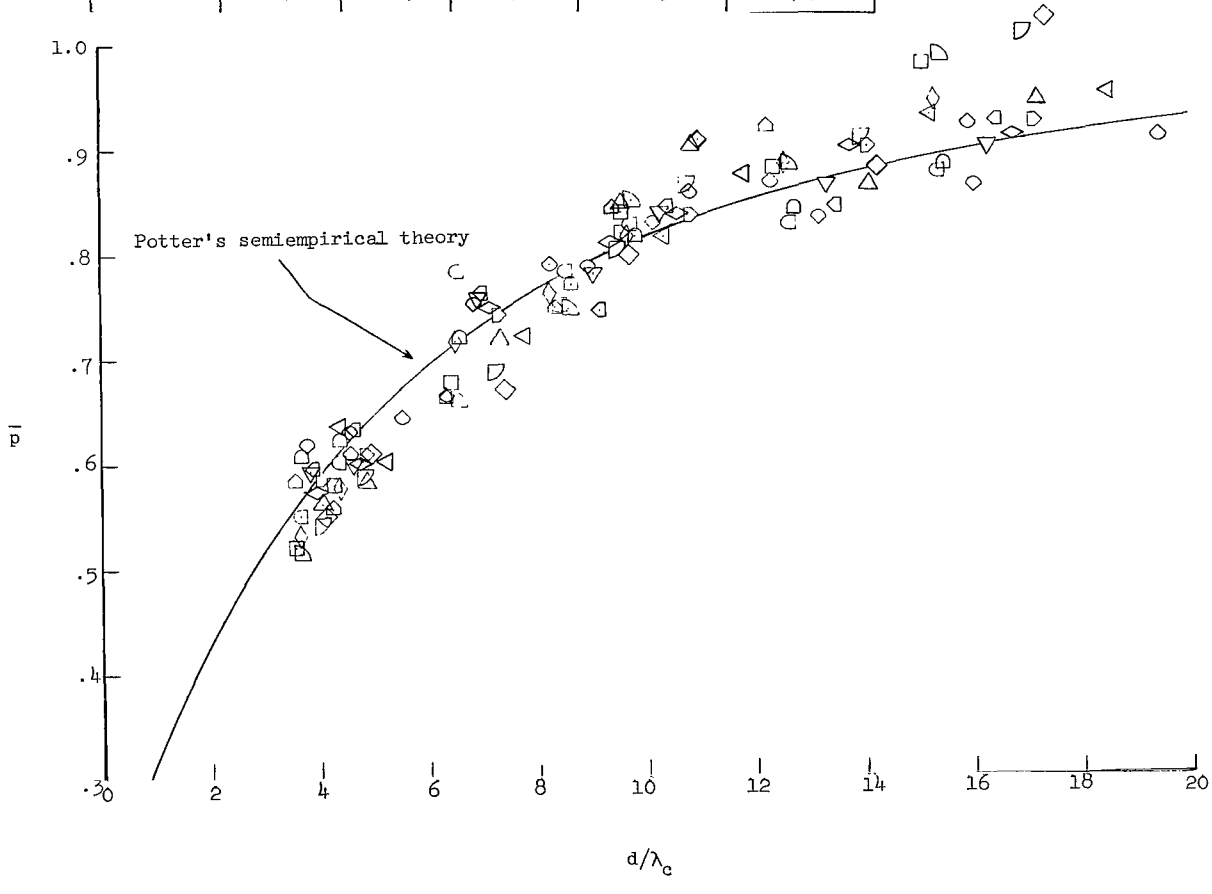

Figure 8.- Experimental and theoretical variation of normalized pressure with orifice size. $T_w \approx 320^0$ K (576^0 R).

that is, on K_w. (See fig. 3.) Thus, the top curve represents the minimum theoretical orifice effect obtainable during the present tests based on the measured values of heat transfer and pressure while the lower curve represents the maximum theoretical orifice effect obtainable. The theoretical curves for all other tests fall between these extremes, the curves being weighted toward the lower curve. It may be noted that much of the data fall below the lower curve over the entire $d/\lambda_{c,i}$ range. However, within the overall accuracy of the present data, figure 7 illustrates agreement between theory and experiment.

Figure 7 also shows that the trend of the nitrogen data and the air data are the same for the conditions involved in the present tests. Agreement with theory is also similar for the two gases.

All the experimental data are shown in figure 8 as normalized pressure $\bar{p}$ plotted against d/λ_c. The average of the experimental data tends to cross the curve obtained from Potter's experiment. Once again, however, the agreement between theory and experiment is reasonable. The scatter of the data in figure 8 appears worse than that in figure 7 because of a scale change and because $\bar{p}$ is more sensitive to changes in p_i than is p_i/p_{io}.

One point that is evident in the present data (figs. 4 to 8) is that the indicated pressure was still increasing for the largest orifice used (diameter = 2.69 mm = 0.106 inch). Thus, it appears that a correction by use of Potter's semiempirical theory is preferable in many cases to the use of extremely large orifices.

CONCLUDING REMARKS

An experimental investigation of the effect of orifice diameter and heat-transfer rate on measured pressures has been made in the region between continuum and free molecule flow. Heat-transfer and pressure measurements were made over a range of tunnel test conditions with Mach number varying from 12.2 to 14.1, free-stream Reynolds number varying from 400 to 889 per centimeter (1.22×10^4 to 2.71×10^4 per foot), free-stream mean-free-path length varying from 0.234 to 0.452 mm (0.0092 to 0.0178 inch), and total enthalpy varying from 3.07 to 4.95 MJ/kg (1320 to 2130 Btu/lbm). Although the data were obtained on a 10° semivertex angle cone with a plane, blunted tip, the results are general when presented in terms of parameters from a previously existing theory.

A consideration of lag time, outgassing, thermal creep, and momentum mixing indicated that the effects of these phenomena on the measured pressures were negligible in comparison with the measured effect. Thus, it is believed that the orifice effect was essentially isolated in the present data.

Potter's semiempirical theory for the orifice effect agreed very well with the experimental data. This was true even though the present tests, which were conducted in both air and nitrogen, extend the range of experimental data obtained on the orifice effect under actual flow conditions. The extension is due to the higher heat-transfer rates obtained at the density level involved.

The trend of the data and the agreement with theory was the same for both the air and nitrogen data. Thus, for the range of variables involved in the present tests, no difference in the orifice effect was noted between the two gases.

In all the tests where there was heat transfer to the model, the measured pressure was still increasing for the largest orifice diameter tested (2.69 mm = 0.106 inch). It is evident that the proper size orifice needed to measure the correct pressure will depend on both the density level and the heat-transfer rate. In many cases, it may be more practical to use an orifice of a reasonable size and correct the pressure data by use of Potter's semiempirical theory than to use the large orifice needed to be free of the orifice effect.

Also, under conditions where the orifice effect may be a factor to be considered in pressure measurements, it is essential to know the heat-transfer rate. Pressure measurements may be made much more reliable by a simultaneous measurement of heat-transfer rate for use in Potter's semiempirical theory.

Langley Research Center,
National Aeronautics and Space Administration,
Langley Station, Hampton, Va., October 6, 1966,
129-01-10-01-23.

APPENDIX A

A METHOD FOR CORRECTING MEASURED PRESSURES FOR SMALL, UNKNOWN, MODEL MISALINEMENT ANGLES THROUGH THE USE OF ALINEMENT ORIFICES

The misalinement correction to the present data was complicated somewhat by the fact that the amount and direction of misalinement was unknown prior to the tests. Thus, the correction which was applied to the pressure data for model misalinement was a first-order correction of the form

$$p' = p_i + C \cos(\phi - \phi_m) \tag{A1}$$

This equation is of the same form as equation (29) of reference 16 and is good only for small misalinement angles. However, comparisons of first- and second-order theory, as presented in reference 19, for the maximum misalinement angle believed possible for the present tests ($\delta = 1^o$) indicated that equation (A1) was adequate for correcting the present data.

In equation (A1), p_i is the zero misalinement cone pressure and, for small misalinement angles, is the pressure on the misalined cone 90^o from the most windward ray; C is a test constant which is dependent on misalinement angle, Mach number, and the cone-semivertex angle, by analogy with equation (29) of reference 16; ϕ is any angular location around the cone circumference, and ϕ_m is the angular location of the most windward conical ray; and p' is the pressure at various angular locations around the circumference of the cone. Because of the orifice effect, p', p_i, and C are functions of orifice diameter in the present tests.

Equation (A1) was written for each alinement orifice ($\phi_A = 0^o$, 120^o, 240^o) and values of $p_{i,A}$, C_A, and ϕ_m for a given test were found by simultaneous solution of the resulting three equations. Next, it was assumed that although an orifice effect on the pressures existed, the nondimensionalized pressure distribution p_i/p' around the circumference of the cone was independent of orifice diameter. Therefore, the misalinement corrections for orifices other than the alinement orifices were made by use of

$$\frac{p_i}{p'} = \frac{p_{i,A}}{p'_A} \tag{A2a}$$

or

$$p_i = \frac{p'}{1 + \frac{C_A}{p_{i,A}} \cos\left(\phi - \phi_m\right)} \tag{A2b}$$

By the use of three alinement orifices, a correction was made to measured pressures on a misalined cone without prior knowledge of the direction or (small) amount of misalinement. The direction of misalinement was found when ϕ_m was calculated. The approximate amount of misalinement may be found from reference 16 by making the assumptions involved in equations (A2). In figure 9, which shows the coordinate system considered in this discussion, δ and ϕ_m are defined. This method is most reliable in regions where surface pressure gradients due to viscous- or bluntness-induced effects are not severe. Alinement orifices located in regions of severe pressure gradient could give erroneous misalinement angles.

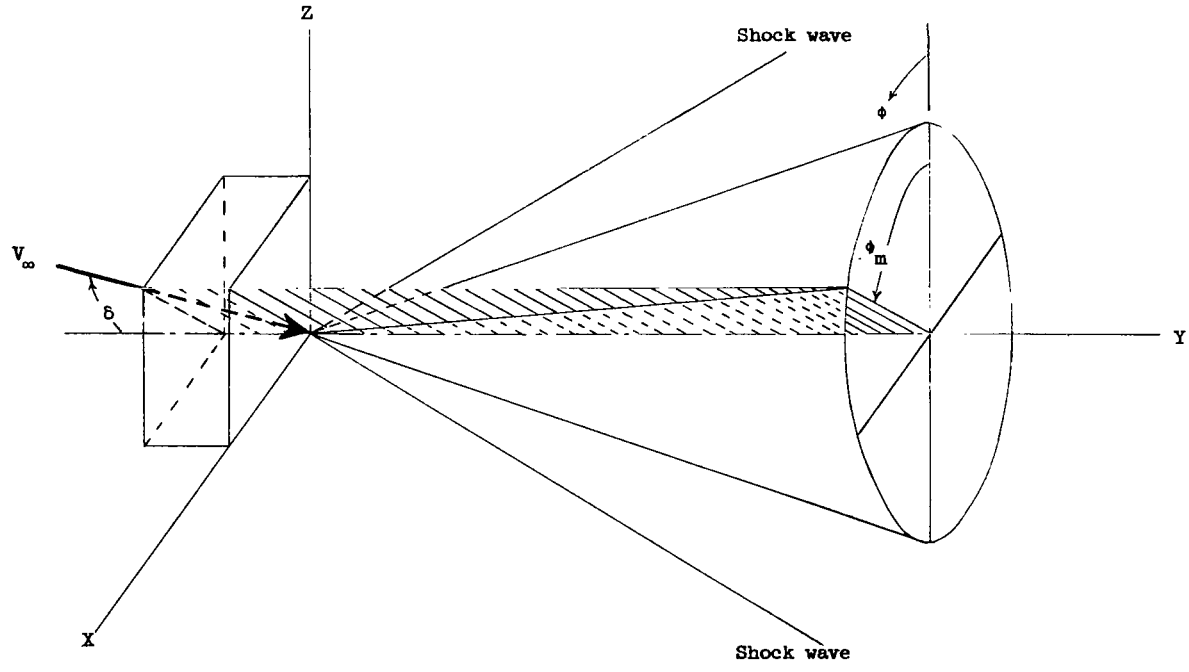

Figure 9.- Body-fixed coordinate system.

According to the pressure distribution correlation for blunted cones shown as figure 5 of reference 20, the present pressure data lie downstream of the overexpansion region caused by the blunt nose of the cone. In this region, bluntness theory indicates that the pressure should be very close to sharp cone pressure.

APPENDIX A

In the usual case, misalinement angles of less than 0.25° were encountered in the present tests. However, if a maximum possible misalinement angle of 1° is assumed for the present tests, figure 5 of reference 20 indicates that any bluntness effects on the apparent misalinement angle should be negligible.

Viscous effects on the pressures just downstream of the overexpansion are more difficult to analyze, but the effects should be small in this region for the present tests. In any event, bluntness and viscous induced pressure effects would be in opposition in any effect on the apparent misalinement angle. Also, the manner in which the misalinement correction is applied inherently corrects for small induced pressure effects.

APPENDIX B

AN EXTENSION OF POTTER'S SEMIEMPIRICAL THEORY FOR THE ORIFICE EFFECT TO LOWER VALUES OF K_w

Potter et al. (ref. 9) have stated the cause of the orifice effect very clearly. The orifice effect is a thermal transpiration or thermomolecular flow type effect; that is, it arises because of the existence of unequal speed distributions between incoming and outgoing particles in the orifice entrance region. The effect on the pressure inside the orifice cavity is that for a given heat-transfer rate and density level (between continuum and free molecule), the indicated pressure decreases as orifice size decreases.

The equilibrium condition for orifice flow in all regions is that the net mass flux across the orifice face be zero. In the case of free molecule flow, this condition for equilibrium leads to the result that a pressure differential must counterbalance the temperature differential. In the continuum case, the condition of no net mass flow leads to the result that the pressure gradient be zero. Logically, the intermediate regions must show a smooth transition as has been demonstrated experimentally by Potter et al. (ref. 9).

Potter et al. used their correlation of experimental data (obtained in a bell jar) to formulate a working chart for the correction of the orifice effect in terms of p_i/p_{io}, $d/\lambda_{c,i}$, and K_w. However, the range of K_w covered on this chart was not low enough to permit it to be used in comparing the present data with the semiempirical theory. Thus, it became necessary to extend the usability of the semiempirical theory presented in reference 9.

In order to accomplish this extension, an analytical expression between the normalized pressure, $\bar{p}$, and d/λ_c was needed. Figure 9 of reference 9 presents $\bar{p}$ plotted against d/λ_c in argon and figure 10 of that report presents $\bar{p}$ plotted against d/λ_c in nitrogen. The faired curves through the experimental data in these two figures are identical. A curve fit to the faired curve yielded, for $0.5 < d/\lambda_c < 22$,

$$\bar{p} = 1 - \frac{1}{\left(0.071 \frac{d}{\lambda_c} + 1.068\right)^{2.95}} \tag{B1}$$

where $\bar{p}$ is the normalized pressure which has been defined previously (ref. 9) as

$$\bar{p} = \frac{p_i/p_{io} - \left(p_i/p_{io}\right)_L}{1 - \left(p_i/p_{io}\right)_L} \tag{B2}$$

where $\left(p_i/p_{io}\right)_L$ is the ratio of pressure in the limit of free molecule flow to true pressure and p_i/p_{io} is the ratio of pressure at a given Knudsen number to true pressure. Combining equations (B1) and (B2) yields

$$\left(\frac{p_i}{p_{io}}\right)_L = 1 + D\left(\frac{p_i}{p_{io}} - 1\right) \tag{B3}$$

where

$$D = \left(0.071\,\frac{d}{\lambda_c} + 1.068\right)^{2.95} \tag{B4}$$

Combining equations (19) and (20) of reference 9 gives the following relation between limiting pressure ratio, heat-transfer rate, true pressure, and wall temperature:

$$\dot{q}_w = \frac{0.8512\gamma p_{io}\left(RT_w\right)^{0.5}}{N_{Pr,w}(\gamma - 1)}\left[\frac{\left(p_i/p_{io}\right)_L - 1}{\left(p_i/p_{io}\right)_L}\right] \tag{B5}$$

Defining

$$B = \frac{\dot{q}_w N_{Pr,w}(\gamma - 1)}{0.8512\gamma\left(RT_w\right)^{0.5}} \tag{B6}$$

and solving equation (B5) for the limiting pressure ratio yields

$$\left(\frac{p_i}{p_{io}}\right)_L = \frac{p_{io}}{p_{io} - B} \tag{B7}$$

Equating equations (B3) and (B7) eliminates $\left(p_i/p_{io}\right)_L$ and gives

$$p_{io}^2 + \left(\frac{B}{D} - B - p_i\right)p_{io} + Bp_i = 0 \tag{B8}$$

Solving equation (B8) for p_{io} gives the true pressure as

$$p_{io} = \frac{-\left(\frac{B}{D} - B - p_i\right) + \sqrt{\left(\frac{B}{D} - B - p_i\right)^2 - 4Bp_i}}{2} \tag{B9}$$

The known quantities in equation (B9) are p_i and B, while d/λ_c and therefore D are unknown. Consequently, equation (B9) must be solved by iteration and $d/\lambda_{c,i}$ may be used as a first choice of d/λ_c.

Equation (B8) may be solved for p_i to yield

$$p_i = p_{io} + \frac{Bp_{io}}{D\left(p_{io} - B\right)} \tag{B10}$$

Equation (B10) is valuable as a means of predicting the magnitude of orifice effect on pressure measurements.

In many cases, it may be desirable to determine the orifice size necessary to maintain the indicated pressure within a certain percentage of the true pressure, that is,

$$p_i = Ap_{io} \tag{B11}$$

where A is the desired percentage. Substitution of equation (B11) into equation (B10) yields

$$d = 14.1\left\{\left[\frac{B}{\left(p_{io} - B\right)(A - 1)}\right]^{0.339} - 1.068\right\}\lambda_c \tag{B12}$$

for the proper orifice diameter.

Equation (B8) may also be used to derive a working chart for the correction of the orifice effect as is shown in figure 11 of reference 9. By letting

$$K_w = 0.8512\,\frac{B}{p_i} \tag{B13}$$

and

$$\frac{d}{\lambda_c} = \frac{d}{\lambda_{c,i}}\,\frac{p_{io}}{p_i} \tag{B14}$$

equation (B8) can be rearranged to give

$$K_w = 0.8512 \frac{p_{io}}{p_i}\left[1 - \frac{1}{1 + \left(0.071 \frac{d}{\lambda_{c,i}} \frac{p_{io}}{p_i} + 1.068\right)^{2.95}\left(\frac{p_i}{p_{io}} - 1\right)}\right] \tag{B15}$$

By choosing a range of p_i/p_{io}, equation (B15) may be used to calculate a range of K_w for a given value of $d/\lambda_{c,i}$. Figure 3 of this report represents an extended correction chart for orifice effects obtained by this method.

REFERENCES

1. Sinclair, Archibald R.; and Robins, A. Warner: A Method for the Determination of the Time Lag in Pressure Measuring Systems Incorporating Capillaries. NACA TN 2793, 1952.

2. Maslach, George J.: Some Problems Associated With the Measurement of Very Low Pressures. AGARD Rept. 175, Mar. 1958.

3. Knudsen, Martin: Thermischer Molekulardruck in Röhren. Annalen der Physik, vol. 83, 1910, pp. 797-821.

4. Howard, Weston M: An Experimental Investigation of Pressure Gradients Due to Temperature Gradients in Small Diameter Tubes. Aeron. Lab., GALCIT Memo. No. 27 (Contract DA-04-495-Ord-19), June 10, 1955.

5. Arney, G. D., Jr.; and Bailey, A. B.: An Investigation of the Equilibrium Pressure Along Unequally Heated Tubes. AEDC-TDR-62-26, U.S. Air Force, Feb. 1962.

6. Arney, G. D., Jr.; and Bailey, A. B.: Addendum to an Investigation of the Equilibrium Pressure Along Unequally Heated Tubes. AEDC-TDR-62-188, U.S. Air Force, Oct. 1962.

7. Talbot, L.: Viscosity Corrections to Cone Probes in Rarefied Supersonic Flow at Nominal Mach Number of 4. NACA TN 3219, 1954.

8. Rayle, Roy E., Jr.: An Investigation of the Influence of Orifice Geometry on Static Pressure Measurements. M. S. Thesis, M.I.T., 1949.

9. Potter, J. Leith; Kinslow, Max; and Boylan, David E.: An Influence of the Orifice on Measured Pressures in Rarefied Flow. AEDC-TDR-64-175, U.S. Air Force, Sept. 1964.

10. Bailey, A. B.; and Boylan, D. E.: Some Experiments on Impact-Pressure Probes in a Low-Density, Hypervelocity Flow. Proc. 1962 Heat Transfer Fluid Mech. Inst., Stanford Univ. Press, F. Edward Ehlers, James J. Kauzlarich, Charles A. Sleicher, Jr., and Robert E. Street, eds., 1962, pp. 62-75.

11. Bailey, A. B.: Further Experiments on Impact-Pressure Probes in a Low-Density, Hypervelocity Flow. AEDC-TDR-62-208, U.S. Air Force, Nov. 1962.

12. Vidal, R. J.; and Bartz, J. A.: Experimental Studies of Low-Density Effects in Hypersonic Wedge Flows. Rept. No. AF 1500-A-2 (AFOSR 65-0335), Cornell Aero. Lab., Inc., Dec. 1964.

13. Deskins, H. Eugene; and Boylan, David E.: Pressure Orifice Shape Effect in Rarefied Flow With Heat Transfer. AIAA J., vol. 3, no. 5, May 1965, pp. 956-957.

14. Boatright, W. B.; Stewart, R. B.; and Sebacher, D. I.: Testing Experience and Calibration Experiments in a Mach Number 12, 1-Foot Hypersonic Arc Tunnel. Paper presented at Third Hypervelocity Techniques Symposium (Denver, Colorado), Mar. 1964.

15. Vitkus, P. L.: A Multi-Point Vacuum Measuring System for Low Pressure Wind Tunnels. 1959 Sixth Nat. Symposium on Vacuum Tech., Trans., C. Robert Meissner, ed., Pergamon Press (New York), 1960, pp. 89-93.

16. Staff of the Computing Section, Center of Analysis (Under Direction of Zdeněk Kopal): Tables of Supersonic Flow Around Yawing Cones. Tech. Rep. No. 3 (NOrd Contract No. 9169), M.I.T., 1947.

17. Goldsmith, Alexander; Hirschhorn, Harry J.; and Waterman, Thomas E.: Thermophysical Properties of Solid Materials. Vol. II – Alloys (Melting Temperature Above 1000° F). WADC Tech. Rept. 58-476, Vol. II, U.S. Air Force, Nov. 1960.

18. Sebacher, Daniel I.: Flow Visualization Using an Electron Beam Afterglow In N_2 and Air. AIAA J., vol. 4, no. 10, Oct. 1966, pp. 1858-1859.

19. Roberts, Richard C.; and Riley, James D.: A Guide to the Use of the M.I.T. Cone Tables. J. Aeron. Sci., vol. 21, no. 5, May 1954, pp. 336-342.

20. Griffith, B. J.; and Lewis, Clark H.: A Study of Laminar Heat Transfer to Spherically Blunted Cones and Hemisphere-Cylinders at Hypersonic Conditions. AEDC-TDR-63-102 (Contract No. AF 40(600)-1000), Arnold Eng. Dev. Center, June 1963.

TABLE I.- TEST CONDITIONS

Test	$p_{t,1}$		H_t		$p_{t,2}$		M_∞	$N_{Re,\infty}$		λ_∞		h_w/H_t	$\dot{q}_w$	
	N/cm^2	atm	MJ/kg	Btu/lbm	N/cm^2	mm Hg		per cm	per ft	mm	in.		J/cm^2-s	Btu/ft^2-sec
Air														
1	61	6.0	0.30	127	0.024	1.80	----	---	---------	-----	------	1.004	≈0	≈0
2	189	18.7	4.23	1820	.100	7.51	12.2	400	1.22×10^4	0.452	0.0178	.075	-8.09	-7.12
3	240	23.7	4.37	1880	.115	8.63	12.4	449	1.37	.406	.0160	.073	-6.72	-5.92
4	249	24.6	4.47	1920	.115	8.63	12.4	436	1.33	.419	.0165	.071	-6.39	-5.63
5	223	22.0	4.35	1870	.117	8.78	12.2	449	1.37	.401	.0158	.074	-8.15	-7.18
6	224	22.1	3.51	1510	.101	7.58	13.1	617	1.88	.315	.0124	.089	-7.42	-6.53
7	239	23.6	4.09	1760	.102	7.64	12.9	476	1.45	.401	.0158	.078	-9.45	-8.32
8	286	28.2	3.07	1320	.102	7.61	14.1	889	2.71	.234	.0092	.103	-8.15	-7.18
9	261	25.8	3.56	1530	.108	8.08	13.3	666	2.03	.297	.0117	.090	-9.31	-8.20
10	214	21.1	4.02	1730	.114	8.54	12.3	499	1.52	.366	.0144	.080	-8.72	-7.68
11	236	23.3	4.02	1730	.121	9.10	12.4	538	1.64	.343	.0135	.080	-9.72	-8.56
12	259	25.6	4.14	1780	.121	9.10	12.6	531	1.62	.351	.0138	.078	-9.65	-8.50
13	250	24.7	4.37	1880	.118	8.88	12.4	463	1.41	.399	.0157	.075	-12.48	-10.99
Nitrogen														
14	234	23.1	4.00	1720	0.101	7.60	13.7	571	1.74×10^4	0.356	0.0140	0.078	-4.83	-4.25
15	215	21.2	4.23	1820	.114	8.55	13.1	538	1.64	.358	.0141	.076	-8.98	-7.91
16	256	25.3	4.95	2130	.141	10.58	12.7	502	1.53	.376	.0148	.066	-11.71	-10.31
17	248	24.5	4.33	1860	.106	7.92	13.6	522	1.59	.386	.0152	.075	-8.38	-7.38

TABLE II.- EXPERIMENTAL PRESSURE DATA

(a) Air

d,mm	ϕ, deg	Pressure, N/m^2, for test – 1		2		3		4		5		6	
		Uncorrected	Corrected	Uncorrected	Corrected	Uncorrected	Corrected	Uncorrected	Corrected	Uncorrected	Corrected	Uncorrected	Corrected
0.64	30	13.6	13.1	25.7	28.8	32.0	35.6	36.7	35.9	34.4	34.0	30.1	29.9
.76	60	14.0	13.9	29.1	30.3	34.3	36.1	38.0	37.3	36.1	35.2	30.4	31.1
1.14	160	12.8	13.7	37.6	32.7	44.0	39.5	38.3	38.8	38.7	37.9	33.7	35.5
1.50	200	12.5	13.2	38.8	34.5	46.9	42.7	40.9	41.9	40.8	41.1	34.8	35.5
1.70	0	14.9	14.0	31.2	36.7	38.7	44.0	45.3	44.5	42.3	42.7	37.9	36.5
1.70	120	13.3	14.0	40.3	36.7	47.1	44.0	44.4	44.5	44.1	42.7	34.5	36.5
1.70	240	13.9	14.0	38.4	36.7	46.4	44.0	43.7	44.5	41.5	42.7	37.3	36.5
2.21	280	13.2	12.8	35.3	37.7	41.7	43.1	43.6	43.9	42.3	43.9	38.4	36.5
2.69	320	14.0	13.2	34.7	40.1	40.7	45.1	47.7	47.3	45.1	46.4	39.9	37.7
2.57	Tip	240		1001		1151		1151		1171		1011	
δ, deg		----	0	0.92	0	0.74	0	0.13	0	0.23	0	0.35	0
ϕ_m, deg		341		169		176		25		103		309	

d, inch	ϕ, deg	Pressure, mm Hg, for test – 1		2		3		4		5		6	
		Uncorrected	Corrected	Uncorrected	Corrected	Uncorrected	Corrected	Uncorrected	Corrected	Uncorrected	Corrected	Uncorrected	Corrected
0.025	30	0.102	0.098	0.193	0.216	0.240	0.267	0.275	0.269	0.258	0.255	0.226	0.224
.030	60	.105	.104	.218	.227	.257	.271	.285	.280	.271	.264	.228	.233
.045	160	.096	.103	.282	.245	.330	.296	.287	.291	.290	.284	.253	.266
.059	200	.094	.099	.291	.259	.352	.320	.307	.314	.306	.308	.261	.266
.067	0	.112	.105	.234	.275	.290	.330	.340	.334	.317	.320	.284	.274
.067	120	.100	.105	.302	.275	.353	.330	.333	.334	.331	.320	.259	.274
.067	240	.104	.105	.288	.275	.348	.330	.328	.334	.311	.320	.280	.274
.087	280	.099	.096	.265	.283	.313	.323	.327	.329	.317	.329	.288	.274
.106	320	.105	.099	.260	.301	.305	.338	.358	.355	.338	.348	.299	.283
.101	Tip	1.80		7.51		8.63		8.63		8.78		7.58	
δ, deg		-----	0	0.92	0	0.74	0	0.13	0	0.23	0	0.35	0
ϕ_m, deg		341		169		176		25		103		309	

d,mm	ϕ, deg	Pressure, N/m^2, for test – 7		8		9		10		11		12		13	
		Uncorrected	Corrected	Uncorrected	Corrected	Uncorrected	Corrected	Uncorrected	Corrected	Uncorrected	Corrected	Uncorrected	Corrected	Uncorrected	Corrected
0.64	30	31.1	29.1	34.7	33.2	34.1	33.5	33.2	33.3	34.1	33.5	35.1	35.1	43.2	41.2
.76	60	33.6	30.3	34.5	33.5	34.9	34.5	33.7	33.5	35.2	34.3	35.7	35.7	44.1	42.4
1.14	160	35.2	34.0	35.6	36.7	37.3	38.1	38.3	37.7	38.7	38.5	39.6	39.6	45.7	47.5
1.50	200	33.3	35.2	36.0	37.6	36.9	37.7	38.5	38.4	39.7	40.3	41.9	41.9	47.6	50.0
1.70	0	37.5	37.1	40.1	38.7	41.3	40.4	39.5	39.9	41.3	41.1	42.5	42.5	52.5	50.3
1.70	120	40.9	37.1	38.5	38.7	40.0	40.4	40.5	39.9	41.9	41.1	42.3	42.3	50.0	50.3
1.70	240	32.9	37.1	37.3	38.7	39.9	40.4	39.6	39.9	40.0	41.1	42.3	42.3	48.3	50.3
2.21	280	33.9	38.5	38.4	38.8	40.5	40.4	40.0	40.7	41.9	42.9	44.3	44.3	51.6	52.3
2.69	320	37.2	40.1	40.3	39.6	43.3	42.7	40.9	41.6	42.7	43.2	44.9	44.9	52.8	51.7
2.57	Tip	1019		1015		1077		1139		1213		1213		1184	
δ, deg		0.76	0	0.25	0	0.14	0	0.10	0	0.17	0	0	0	0.30	0
ϕ_m, deg		86		25		5		127		76		---		24	

d, inch	ϕ, deg	Pressure, mm Hg, for test – 7		8		9		10		11		12		13	
		Uncorrected	Corrected	Uncorrected	Corrected	Uncorrected	Corrected	Uncorrected	Corrected	Uncorrected	Corrected	Uncorrected	Corrected	Uncorrected	Corrected
0.025	30	0.233	0.218	0.260	0.249	0.256	0.251	0.249	0.249	0.256	0.251	0.263	0.263	0.324	0.309
.030	60	.252	.227	.259	.251	.262	.259	.253	.251	.264	.257	.268	.268	.331	.318
.045	160	.264	.255	.267	.275	.280	.286	.287	.283	.290	.289	.297	.297	.343	.356
.059	200	.250	.264	.270	.282	.277	.283	.289	.288	.298	.302	.314	.314	.357	.375
.067	0	.281	.278	.301	.290	.310	.303	.296	.299	.310	.308	.319	.319	.394	.377
.067	120	.307	.278	.289	.290	.300	.303	.304	.299	.314	.308	.317	.317	.375	.377
.067	240	.247	.278	.280	.290	.299	.303	.297	.299	.300	.308	.317	.317	.362	.377
.087	280	.254	.289	.288	.291	.304	.303	.300	.305	.314	.322	.332	.332	.387	.392
.106	320	.279	.301	.302	.297	.325	.320	.307	.312	.320	.324	.337	.337	.396	.388
.101	Tip	7.64		7.61		8.08		8.54		9.10		9.10		8.88	
δ, deg		0.76	0	0.25	0	0.14	0	0.10	0	0.17	0	0	0	0.30	0
ϕ_m, deg		86		25		5		127		76		---		24	

TABLE II.- EXPERIMENTAL PRESSURE DATA – Concluded

(b) Nitrogen

d, mm	ϕ, deg	Pressure, N/m^2, for test –							
		14		15		16		17	
		Uncorrected	Corrected	Uncorrected	Corrected	Uncorrected	Corrected	Uncorrected	Corrected
0.64	30	31.2	30.3	31.7	31.2	39.1	38.7	32.0	29.9
.76	60	----	----	31.9	31.6	37.7	37.6	31.2	29.2
1.14	160	32.1	33.1	33.5	34.1	40.8	41.5	30.8	31.9
1.50	200	33.7	34.8	34.8	35.5	44.0	44.5	31.7	34.0
1.70	0	38.0	36.8	37.5	36.7	47.1	46.4	38.3	36.3
1.70	120	36.3	36.8	36.3	36.7	45.9	46.4	36.9	36.3
1.70	240	36.1	36.8	36.4	36.7	46.3	46.4	33.9	36.3
2.21	280	37.6	37.5	37.5	37.3	48.7	48.3	36.8	38.3
2.69	320	40.3	39.5	39.1	38.4	49.7	48.9	----	----
2.57	Tip	1013		1136		1411		1056	
δ, deg		0.20	0	0.13	0	0.09	0	0.44	0
ϕ_m, deg . . .		4		354		341		43	

d, inch	ϕ, deg	Pressure, mm Hg, for test –							
		14		15		16		17	
		Uncorrected	Corrected	Uncorrected	Corrected	Uncorrected	Corrected	Uncorrected	Corrected
0.025	30	0.234	0.227	0.238	0.234	0.293	0.290	0.240	0.224
.030	60	-----	-----	.239	.237	.283	.282	.234	.219
.045	160	.241	.248	.251	.256	.306	.311	.231	.239
.059	200	.253	.261	.261	.266	.330	.334	.238	.255
.067	0	.285	.276	.281	.275	.353	.348	.287	.273
.067	120	.272	.276	.272	.275	.344	.348	.277	.273
.067	240	.271	.276	.273	.275	.347	.348	.254	.273
.087	280	.282	.281	.281	.280	.365	.362	.276	.287
.106	320	.302	.296	.293	.288	.373	.367	-----	-----
.101	Tip	7.60		8.52		10.58		7.92	
δ, deg		0.20	0	0.13	0	0.09	0	0.44	0
ϕ_m, deg . .		4		354		341		43	

"The aeronautical and space activities of the United States shall be conducted so as to contribute . . . to the expansion of human knowledge of phenomena in the atmosphere and space. The Administration shall provide for the widest practicable and appropriate dissemination of information concerning its activities and the results thereof."

—NATIONAL AERONAUTICS AND SPACE ACT OF 1958

NASA SCIENTIFIC AND TECHNICAL PUBLICATIONS

TECHNICAL REPORTS: Scientific and technical information considered important, complete, and a lasting contribution to existing knowledge.

TECHNICAL NOTES: Information less broad in scope but nevertheless of importance as a contribution to existing knowledge.

TECHNICAL MEMORANDUMS: Information receiving limited distribution because of preliminary data, security classification, or other reasons.

CONTRACTOR REPORTS: Technical information generated in connection with a NASA contract or grant and released under NASA auspices.

TECHNICAL TRANSLATIONS: Information published in a foreign language considered to merit NASA distribution in English.

TECHNICAL REPRINTS: Information derived from NASA activities and initially published in the form of journal articles.

SPECIAL PUBLICATIONS: Information derived from or of value to NASA activities but not necessarily reporting the results of individual NASA-programmed scientific efforts. Publications include conference proceedings, monographs, data compilations, handbooks, sourcebooks, and special bibliographies.

Details on the availability of these publications may be obtained from:

SCIENTIFIC AND TECHNICAL INFORMATION DIVISION

NATIONAL AERONAUTICS AND SPACE ADMINISTRATION

Washington, D.C. 20546